Improvement of dynamic range and repeatability in refractive-index-sensing optical comb by combination of saturable-absorber-mirror mode-locking with intracavity multi-mode interference fiber sensor

Ryo Oe[1,2], Takeo Minamikawa[2,3,4], Shuji Taue[5], Takuya Nakahara[1], Hidenori Koresawa[1,2], Takahiko Mizuno[2,3,4], Masatomo Yamagiwa[2,3,4], Yasuhiro Mizutani[2,6], Hirotsugu Yamamoto[2,7], Tetsuo Iwata[2,4], Yoshiaki Nakajima[2,8], Kaoru Minoshima[2,3,8], and Takeshi Yasui[2,3,4*]

[1]*Graduate School of Advanced Technology and Science, Tokushima University, Tokushima, Tokushima 770-8506, Japan*

[2]*JST, ERATO, MINOSHIMA Intelligent Optical Synthesizer Project, Tokushima, Tokushima 770-8506, Japan*

[3]*Institute of Post-LED Photonics (pLED), Tokushima University, Tokushima, Tokushima 770-8506, Japan*

[4]*Graduate School of Technology, Industrial and Social Sciences, Tokushima University, Tokushima, Tokushima 770-8506, Japan*

[5]*Electronic and Photonic Systems Engineering Course, Kochi University of Technology, 2-22 Eikokuji, Kochi, Kochi 780-8515, Japan*

[6]*Graduate School of Engineering, Osaka University, 2-1, Yamadaoka, Suita, Osaka 565-0871, Japan*

[7]*Center for Optical Research and Education, Utsunomiya University, 7-1-2, Yoto, Utsunomiya, Tochigi 321-8585, Japan*

[8]*Graduate School of Informatics and Engineering, The University of Electro-Communications, 1-5-1*

E-mail: yasui.takeshi@tokushima-u.ac.jp

Mode-locked fiber comb equipped with multi-mode-interference fiber sensor functions as high-precision refractive-index (RI) sensor benefitting from precise radio-frequency measurement. However, its dynamic range and repeatability are hampered by inherent characteristics in nonlinear-polarization-rotation mode-locking oscillation. In this article, we

introduce saturable-absorber-mirror mode-locking for RI sensing with wide dynamic range and high repeatability. While the RI dynamic range was expanded to 41.4 dB due to high robustness to cavity disturbance, self-starting capability without the need for polarization control improves the RI sensing repeatability to 1.10×10^{-8} every mode-locking activation. Improved dynamic range and repeatability will be useful for enhanced performance of RI sensing.

Refractive index (RI) is an important physical quantity of materials. Therefore, RI sensing has been widely used for identification or characterization of materials. Among various RI sensors, RI fiber sensor benefits from compactness, simplicity, flexibility, noise-robustness, and availability in various environment, and hence has been used for various applications; examples include ethanol sensing,[1] glucose sensing,[2] bio-sensing,[3] and gas sensing.[4] In most case, a change of sample RI is converted into a shift of optical spectrum via the surface plasmon resonance (SPR)[5-8] or the multi-mode interference (MMI).[9-11] However, the precision of RI sensing is limited by the sharpness of optical spectrum dip or peak and/or instrumentational resolution.

If a change of sample RI is transferred into a photonic radio-frequency (RF) signal together with the sharpened spectrum, the RI sensing benefits from high precision, high functionality, convenience, and low cost by making use of frequency standards and precise measurement apparatuses in RF region. Such photonic RF fiber sensor has been effectively applied for strain sensing[12] and ultrasound sensing[13,14] by use of multiple-longitudinal-mode or multiple-polarization-mode spacing in a continuous-wave (CW) fiber laser or a CW fiber-Bragg-grating (FBG) laser. However, inherent frequency fluctuation of mode spacing hampers high-precision RI sensing.

Recently, an optical frequency comb (OFC) appeared as a new photonic RF fiber sensor for liquid RI[15] as well as strain,[16] acoustic wave,[17] and ultrasound.[18] Although OFC has been widely used for an optical frequency ruler secured by a frequency standard,[19-21] OFC was here used for a photonic RF converter of a sample RI change into an OFC mode spacing f_{rep} via a combination of RI-dependent tunable bandpass filtering of an intracavity MMI fiber sensor and wavelength dispersion of a cavity fiber. Due to the ultra-narrow linewidth and high stability in the mode-locking oscillation, this MMI-OFC enables us to precisely measure the RI-dependent f_{rep} shift by an RF frequency counter synchronized with a rubidium frequency standard, leading to an RI resolution of 4.9×10^{-6} refractive index unit (RIU) and an RI accuracy of 5.4×10^{-5} RIU.

One problem of the previous MMI-OFC is in the limited dynamic range and the low repeatability of RI sensing, which are caused by the non-linear polarization rotation (NPR)[22] used for a mode-locking oscillation in the MMI-OFC. Although NPR has been widely used for the fiber-based optical comb with broad optical bandwidth, it is less robust to the external disturbance to the cavity because of high sensitivity to the fiber birefringence. In the MMI-OFC, a large change of the sample RI causes the change

of the intracavity polarization condition via the intracavity MMI fiber sensor, leading to the non-negligible disturbance to the cavity and the disruption of mode-locking oscillation. This is the reason for the limited dynamic range of RI sensing. On the other hand, NPR-based mode-locking oscillation is activated by polarization adjustment in the fiber cavity with a polarization controller. While such polarization adjustment enables flexible mode-locking oscillation, f_{rep} changes every mode-locking activation, leading to its low repeatability. If high repeatability of f_{rep} can be achieved in RI-sensing MMI-OFC, the RI sensing repeatability will be enhanced.

To overcome the limited dynamic range and the low repeatability of RI sensing, robust, less degree of freedom, mode-locking mechanism is required in the RI-sensing MMI-OFC. One possible candidate for such purpose is mode-locking oscillation with saturable absorber mirror (SAM)[23]. SAM enables the easy, stable, and robust mode-locking oscillation without the need for polarization control. While such characteristics in SAM enable us to expand the dynamic range of RI sensing in MMI-OFC, the less degree of freedom mode-locking oscillation will contribute to high repeatability of f_{rep} and RI sensing. In this article, we evaluate the validity of SAM-based MMI-OFC (SAM-MMI-OFC) by comparing with the previous NPR-based MMI-OFC (NPR-MMI-OFC).

Figure 1(a) shows the principle of operation for MMI-OFC.[15] MMI-OFC has a ring-type fiber cavity containing a mode-locker and a MMI fiber sensor. Such the intracavity MMI fiber sensor functions as an RI-dependent tunable optical bandpass filter (bandpass center wavelength = λ_{MMI}) via the multi-mode interference and the Goos-Hänchen shift on the surface of the MMI fiber sensor. In other words, the intracavity MMI fiber sensor shifts the optical spectrum (λ_{MMI}) of the MMI-OFC depending on the sample RI. The wavelength-shifted MMI-OFC spectrum experiences the wavelength dispersion of the cavity fiber, resulting in the conversion from the RI-dependent optical spectral shift to an RI-dependent shift of the optical cavity length nL. Since f_{rep} of OFC is given by c/nL, where c is the velocity of light in vacuum, RI change of a sample can be read out as RI-dependent f_{rep} shift (Δf_{rep}).

We modified a mode-locked Er:fiber laser oscillator for the SAM-MMI-OFC as shown in Fig. 1(b). This oscillator had a ring cavity including a 3.3 m length of single-mode fiber (SMF, SMF-28, Corning, dispersion at 1550 nm = 17 ps/km/nm), a 0.5 m length of erbium-doped fiber (EDF, ER80-4/125, LIEKKI, dispersion at 1550 nm = -65 ps/km/nm), a fiber-coupled saturable absorbed mirror (FC-SAM, SAM-1550-4-4ps-FC, BATOP, high reflection band = 1480~1580 nm, absorbance = 4 %, modulation depth = 2.4 %,

relaxation time constant ~ 4 ps, mounted on a 1 m SMF cable with FC connector), a polarization-insensitive isolator (ISO, PSSI-55-P-I-N-B-I, AFR), a 70:30 fiber coupler (FC, SBC-1-55-30-1-B-1, AFR), a wavelength-division-multiplexing coupler (WDM, WDM-1-9855-1-L-1-F, AFR), a pumping laser diode (pump LD, BL976-PAG900, Thorlabs, wavelength = 980 nm, power = 900 mW), a fiber circulator (FCIR-55-1-B-1-1, AFR), and an intracavity MMI fiber sensor. The intracavity MMI fiber sensor was composed of a clad-less MMF (FG125LA, Thorlabs, core diameter = 125 μm, fiber length = 58 mm) with a pair of SMFs at both ends (core diameter= 6 μm, clad diameter = 125 μm, fiber length = 54 mm), whose detail is given elsewhere.[15] We here set m to 4 for use of the intracavity MMI fiber sensor as the RI-dependent tunable band-pass filter. SAM functions as a stable mode-locker via a fiber circulator. The fiber cavity was enclosed in an aluminum box and its temperature was controlled to 26.0ºC by a combination of a Peltier heater (TEC1-12708, Kaito Denshi, power = 76 W), a thermistor (PB7-42H-K1, Yamaki), and a temperature controller (TED200, Thorlabs, PID control) [not shown in Fig. 1(b)]. The output light from the oscillator was detected by a photodetector (PD), and f_{rep} was measured by an RF frequency counter (53230A, Keysight Technologies, frequency resolution = 12 digit/s) and an RF spectrum analyzer (E4402B, Keysight Technologies, frequency resolution = 1 Hz), both of which were synchronized to a rubidium frequency standard (FS725, Stanford Research Systems, accuracy = 5×10^{-11} and instability = 2×10^{-11} at 1 s). Also, its optical spectrum was measured by an optical spectrum analyzer (AQ6315A, Yokogawa Electric Corp., wavelength accuracy = 0.02 nm, wavelength resolution = 0.02 nm). For comparison, we prepared the NPR-MMI-OFC[15] and enclosed in the same temperature-controlled box. Specification of the NPR-MMI-OFC was set to be similar to the SAM-MMI-OFC as shown later. The same MMI fiber sensor was used in the NPR-MMI-OFC.

Before evaluating the performance of RI sensing, we compared an optical spectrum and an RF spectrum between the SAM-MMI-OFC and NPR-MMI-OFC. Pure water was used here as a liquid sample. Red plot and blue one in Fig. 2 (a) show an optical spectrum of the SAM-MMI-OFC (center wavelength = 1558.8 nm, spectral bandwidth = 0.8 nm, mean power = 1.43 mW) and the NPR-MMI-OFC (center wavelength = 1552.2 nm, spectral bandwidth = 7.7 nm, mean power = 1.46 mW), respectively. The soliton mode-locking oscillation was achieved near the zero-dispersion region of the cavity (-0.0338 ps^2 for the SAM-MMI-OFC and -0.0339 ps^2 for the NPR-MMI-OFC). The spectral bandwidth in the SAM-MMI-OFC was significantly narrower than that in the NPR-MMI-OFC. While the SAM-MMI-OFC can be

easily mode-locked by the narrower spectral light and hence the longer pulse light, the mode-locking oscillation of the NPR-MMI-OFC needs the broader spectral light and the shorter pulse light together with precise polarization control. Such easiness of mode-locking oscillation in the SAM-MMI-OFC will contribute to the robustness to the cavity disturbance caused by the intracavity MMI fiber sensor. Figure 2 (b) compares RF spectrum of f_{rep} between the SAM-MMI-OFC (red plot) and the NPR-MMI-OFC (blue plot), respectively. f_{rep} was 54.86 MHz for the SAM-MMI-OFC and 54.79 MHz for the NPR-MMI-OFC, each of which are approximately equal to each other. Both RF spectra have the similar linewidth around 1 Hz, which is limited by the instrumentational resolution of the RF spectrum analyzer rather than the actual RF spectrum of f_{rep}. We also compare the frequency instability of f_{rep} between the SAM-MMI-OFC and the NPR-MMI-OFC. Red plot and blue one in Fig. 2 (c) show the frequency instability of f_{rep} with respect to the gate time, which is defined as a ratio of f_{rep} fluctuation to the mean f_{rep} value. Little difference was confirmed between them; in other words, use of SAM in MMI-OFC does not degrade the f_{rep} instability and has a potential to achieve the same RI resolution as the NPR-MMI-OFC.

To confirm the RI sensing capability in optical region, we first investigated the RI-dependent λ_{MMI} shift in the SAM-MMI-OFC and NPR-MMI-OFC. Mixtures of ethanol and pure water were used here as a liquid sample. The sample RI was adjusted by changing the mixture ratio between ethanol and water. Furthermore, the temperature of the sample was controlled to 22 ºC by a combination of a K-type thermocouple (TJA-550K, AS ONE), a cord heater (603-60-69-01, Tokyo Glass Kikai, power = 15 W), and a temperature controller (TJA-550, AS ONE, PID control, display resolution = 0.1 ºC). The relationship between the ethanol volume concentration EC (unit: EtOH%) and the sample RI (unit: RIU) is given by $RI = 1.3326+4.90\times10^{-4}\times EC$.[24] The resulting RI-dependent λ_{MMI} shift was determined to be 94.5 nm/RIU for the SAM-MMI-OFC and 67.8 nm/RIU for NPR-MMI-OFC, respectively (not shown). We next evaluated a relation between sample RI and f_{rep} shift (Δf_{rep}) in the SAM-MMI-OFC and NPR-MMI-OFC. Figures 3(a) and 3(b) respectively show the RI-dependent RF spectrum shift of f_{rep} in the SAM-MMI-OFC and the NPR-MMI-OFC for the ethanol/water samples with different mixture ratios (= 0–20 EtOH%, corresponding to 1.333–1.342 RIU), acquired by an RF spectrum analyzer. The amount of spectral shift was significantly larger than the spectral linewidth in both. Then, we measured the RI-dependent Δf_{rep} more precisely by using an RF frequency counter as shown in Fig. 3(c). Although the linear relation was confirmed in the SAM-MMI-OFC and the NPR-MMI-OFC, the former shows the

better linearity than the later. The RF slope coefficient was determined to be -5.82 Hz/EtOH% for the SAM-MMI-OFC and -4.01 Hz/EtOH% for the NPR-MMI-OFC. Since the RF slope coefficient ratio [= (-5.82 Hz/EtOH%)/(-4.01 Hz/EtOH%) = 1.45] significantly agrees with the optical slope coefficient ratio of the SAM-MMI-OFC to the NPR-MMI-OFC [= (94.5 nm/RIU)/(67.8 nm/RIU) = 1.39], difference of the RF slope coefficient between the SAM-MMI-OFC and the NPR-MMI-OFC is mainly due to difference of the optical slope coefficient between. From these slope coefficients and frequency fluctuation of f_{rep}, the RI resolution was determined to be 3.37×10^{-6} for the SAM-MMI-OFC and 6.92×10^{-6} for the NPR-MMI-OFC at a measurement time of 0.5 s.

We further investigated the RI-dependent Δf_{rep} of water/ethanol samples within the wider range of mixture ratio (0−100 EtOH%, corresponding to 1.333–1.382 RIU). Figure 4(a) shows the RI-dependent Δf_{rep} of the water/ethanol sample in the SAM-MMI-OFC. The SAM-based mode-locking oscillation was maintained in all ethanol concentrations. The resulting slope coefficient in the low concentration was larger than that in the high concentration because the RI value of water/ethanol mixture increased in the low concentration (= 0−80 EtOH%), reached the plateau around 80%, and decreased in the high concentration (= 80−100 EtOH %).[11] Figure 4(b) shows the RI-dependent Δf_{rep} of the water/ethanol sample in the NPR-MMI-OFC. In contrast to the SAM-MMI-OFC, the NPR-based mode-locking oscillation was lost four times due to the less robustness to the cavity disturbance caused by the intracavity MMI fiber sensor. When we activated the mode-locking oscillation again by fine adjustment of an intracavity polarization controller, the f_{rep} value was significantly jumped from the f_{rep} value before losing the mode-locking oscillation. As a result, the RI-dependent Δf_{rep} slope shows several discontinuity points. Such discontinuity points hampers the wide dynamic range of RI sensing in the NPR-MMI-OFC. Dynamic range of RI sensing in the SAM-MMI-OFC and the NPR-MMI-OFC is given by

$$DR_{SAM} = 10 \log [(RI_{max} - RI_{min})/(\text{RI resolution})]$$
$$= 10 \log [(1.3792–1.3326)/(3.37\times10^{-6})]= 41.4 \text{ dB} \quad (1)$$
$$DR_{NPR} = 10 \log [(1.3473–1.3326)/(6.92\times10^{-6})]= 33.3 \text{ dB} \quad (2)$$

where RI_{max} and RI_{max} are the maximum and minimum RI values. This comparison clearly indicates the superiority of the SAM-MMI-OFC over the NPR-MMI-OFC for the wide dynamic range of RI sensing. The maximum RI will be limited by the RI of the clad-less MMF (= 1.444 RIU) because the MMI fiber sensor is based on the total reflection at a boundary between the clad-less MMF surface and the sample.

We evaluate the repeatability of f_{rep} in the SAM-MMI-OFC and the NPR-MMI-OFC. Figure 5(a) shows the temporal change of f_{rep} in the SAM-MMI-OFC when the mode-locking oscillation was disrupted by turning the pumping LD off. Due to the self-starting of the mode-locking oscillation without the need for additional adjustment of the intracavity component, f_{rep} values was recovered with high repeatability before and after the disruption. The slow temporal change of f_{rep} was mainly due to the residual thermal drift of nL. However, the temporal behavior of f_{rep} was almost continuous even though the mode-locking oscillation was disrupted. Frequency deviation before and after disruption of mode-locking oscillation was 0.60±0.66 Hz for 4 disruptions, corresponding to the repeatability of $(1.10\pm1.21)\times10^{-8}$ in f_{rep}. This f_{rep} repeatability is equivalent to the repeatability in RI measurement. On the other hand, in NPR-MMI-OFC, it is difficult to activate the mode-locking oscillation as self-starting when the mode-locking oscillation was disrupted by turning the pumping LD off. The NPR-MMI-OFC needs the precise adjustment of the polarization controller for the activation of the mode-locking oscillation. As a result, f_{rep} was jumped with several tens Hz every disruption point even though the scale of the polarization controller was set to that before the disruption, as shown in Fig. 5(b). Frequency deviation before and after disruption of mode-locking oscillation was 46.0±4.67 Hz for 3 disruptions, corresponding to the f_{rep} repeatability of $(8.40\pm0.85)\times10^{-7}$. In this way, the SAM-MMI-OFC has the better repeatability of f_{rep} than the NPR-MMI-OFC.

We here discuss a possibility of the absolute measurement of the sample RI based on one-to-one correspondence between sample RI and f_{rep}. In the previous research of MMI-OFC,[15] the low repeatability of f_{rep} in the NPR-MMI-OFC [see Fig. 5(b)] hampers such absolute RI measurement. Therefore, the relative measurement was performed based on one-to-one correspondence between the sample RI and f_{rep} shift (Δf_{rep}). Use of SAM in MMI-OFC benefits from high repeatability of f_{rep} [see Fig. 5(a)] in addition to wide dynamic range of RI sensing. However, the slow temporal change of f_{rep} was still remained due to the residual thermal drift of nL even though the temperature control of fiber cavity was activated. This remained change will be the last barrier preventing the absolute measurement of the sample RI. One possible method to get rid of this barrier is to compensate the drifted f_{rep} by another measured parameter (for example, carrier-envelope-offset frequency of OFC, optical power, optical spectrum, and so on) related with thermal condition of the fiber cavity. Work is in progress to achieve the absolute measurement of the sample RI based on one-to-one correspondence between sample RI and f_{rep}.

In summary, we proposed use of SAM-based mode-locking, in place of NPR-based mode-locking, in MMI-OFC. Improved dynamic range and repeatability were effectively demonstrated in RI sensing of the ethanol/water sample. While the RI dynamic range was significantly increased due to high robustness to the cavity disturbance caused by the MMI fiber sensor, the self-starting capability without the need for polarization control significantly improves the repeatability of f_{rep}-based RI sensing every mode-locking activation. RI sensing based on SAM-MMI-OFC will be a powerful tool for quality control of liquid products, biosensing, and gas sensing.

This work is supported by Exploratory Research for Advanced Technology (ERATO), Japanese Science and Technology Agency (MINOSHIMA Intelligent Optical Synthesizer Project, JPMJER1304).

References

1) S. K. Srivastava, R. Verma, and B. D. Gupta, Sens. Actuators B Chem. **153**, 194 (2011).
2) S. Binu, V. P. Mahadevan Pillai, V. Pradeepkumar, B. B. Padhy, C. S. Joseph, and N. Chandrasekaran, Mater. Sci. Technol. C **29**, 183 (2009).
3) H. Tazawa, T. Kanie, and M. Katayama, Appl. Phys. Lett. **91**, 113901 (2007).
4) S. Sekimoto, H. Nakagawa, S. Okazaki, K. Fukuda, S. Asakura, T. Shigemori, and S. Takahashi, Sens. Actuators B Chem. **66**, 142 (2000).
5) W. B. Lin, J. M. Chovelon, and N. Jaffrezic-Renault, Appl. Opt. **39**, 3261 (2000).
6) P. Bhatia and B. D. Gupta, Plasmonics **8**, 779 (2013).
7) K. Balaa, M. Kanso, S. Cuenot, T. Minea, and G. Louarn, Sens. Actuators B Chem. **126**, 198 (2007).
8) J. F. Masson, Y. C. Kim, L. A. Obando, W. Peng, and K. S. Booksh, Appl. Spectrosc. **60**, 1241 (2006).
9) Y. Jung, S. Kim, D. Lee, and K. Oh, Meas. Sci. Technol. **17**, 1129 (2006).
10) Q. Wang and G. Farrell, Opt. Lett. **31**, 317 (2006).
11) S. Taue, Y. Matsumoto, H. Fukano, and K. Tsuruta, Jpn. J. Appl. Phys. **51**, 04DG14 (2012).
12) S. Liu, Z. Yin, L. Zhang, L. Gao, X. Chen, and J. Cheng, Opt. Lett. **35**, 835 (2010).
13) T. Guo, A. C. Wong, W. S. Liu, B. O. Guan, C. Lu, and H. Y. Tam, Opt. Express **19**, 2485 (2011).
14) Y. Liang, L. Jin, L. Wang, X. Bai, L. Cheng, and B.-O. Guan, Sci. Rep. **7**, 40849 (2017).
15) R. Oe, S. Taue, T. Minamikawa, K. Nagai, K. Shibuya, T. Mizuno, M. Yamagiwa, Y. Mizutani, H. Yamamoto, T. Iwata, H. Fukano, Y. Nakajima, K. Minoshima, and T. Yasui, Opt. Express **26**, 19694 (2018).
16) T. Minamikawa, T. Ogura, Y. Nakajima, E. Hase, Y. Mizutani, H. Yamamoto, K. Minoshima, and T. Yasui, Opt. Express **26**, 9484 (2018).
17) S. Wang, P. Lu, H. Liao, L. Zhang, D. Liu, and J. Zhang, J. Mod. Opt. **60**, 1892 (2013).
18) T. Minamikawa, T. Masuoka, T. Ogura, K. Shibuya, R. Oe, E. Hase, Y. Nakajima, Y. Yamaoka, T. Mizuno, M. Yamagiwa, Y. Mizutani, H. Yamamoto, T. Iwata, K. Minoshima, and T. Yasui, OSA Continuum **2**, 439 (2019).
19) T. Udem, J. Reichert, R. Holzwarth, and T. W. Hänsch, Opt. Lett. **24**, 881 (1999).
20) M. Niering, R. Holzwarth, J. Reichert, P. Pokasov, T. Udem, M. Weitz, T. W. Hänsch, P. Lemonde, G. Santarelli, M. Abgrall, P. Laurent, C. Salomon, and A. Clairon, Phys. Rev. Lett. **84**, 5496 (2000).

21) T. Udem, R. Holzwarth, and T. W. Hänsch, Nature **416**, 233 (2002).
22) A. Komarov, H. Leblond, and F. Sanchez, Phys. Rev. A **72**, 063811 (2005).
23) B. Ortaç, M. Plötner, J. Limpert, and A. Tünnermann, Opt. Express **15**, 16794 (2007).
24) J. V. Herráez and R. Belda, J. Solution Chem. **35**, 1315 (2006).

Figure Captions

Fig. 1. (a) Principle of operation for MMI-OFC. (b) Experimental setup of SAM-MMI-OFC. Pump LD, pumping laser diode; WDM, wavelength-division-multiplexing coupler; SMF, single-mode fiber; EDF, erbium-doped fiber; SAM module, saturable absorbed mirror module; ISO, polarization-insensitive isolator; FC, 70:30 fiber coupler; PD, photodiode.

Fig. 2. Comparison of (a) optical spectrum, (b) RF spectrum of f_{rep}, and (c) frequency instability of frep between SAM-MMI-OFC and NPR-MMI-OFC.

Fig. 3. RI-dependent frep shift in (a) SAM-MMI-OFC and (b) NPR-MMI-OFC. (c) Relation between ethanol concentration or sample RI and f_{rep} shift (Δf_{rep}) in SAM-MMI-OFC (red plot) and NPR-MMI-OFC (blue plot).

Fig. 4. Relation between ethanol concentration or sample RI and f_{rep} shift (Δf_{rep}) in (a) SAM-MMI-OFC and (b) NPR-MMI-OFC.

Fig. 5. Temporal change of f_{rep} when the mode-locking oscillation was disrupted. (a) SAM-MMI-OFC and (b) NPR-MMI-OFC.

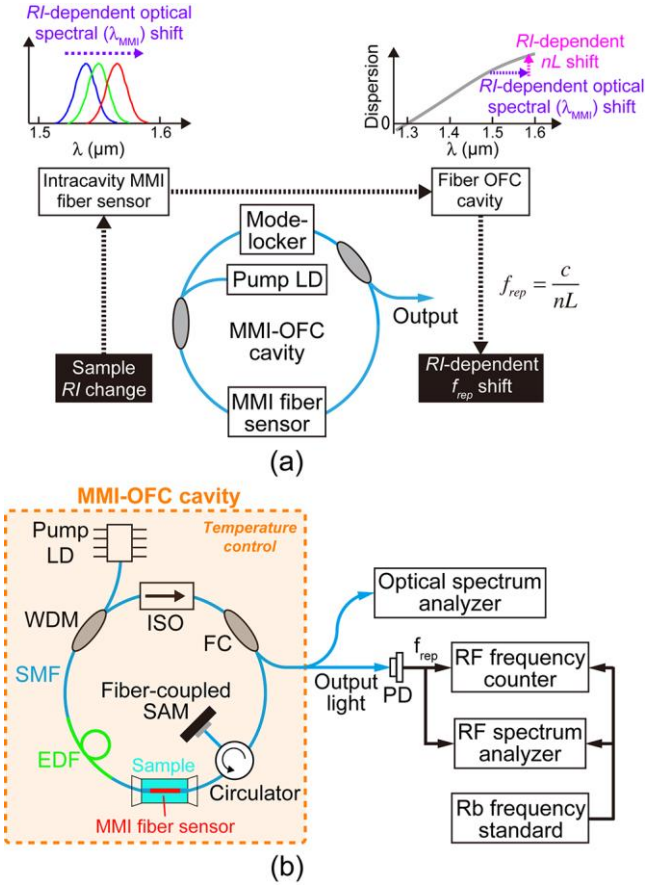
RI-dependent optical spectral (λMMI) shift
1.5
1.6
λ (μm)
Dispersion
0
1.3
1.4
1.5
1.6
λ (μm)
RI-dependent nL shift
RI-dependent optical spectral (λMMI) shift
Intracavity MMI fiber sensor
Fiber OFC cavity
Mode-locker
Pump LD
MMI-OFC cavity
Output
MMI fiber sensor
Sample RI change
RI-dependent frep shift
frep = c/nL
(a)
MMI-OFC cavity
Pump LD
Temperature control
WDM
ISO
FC
SMF
Fiber-coupled SAM
EDF
Sample
Circulator
MMI fiber sensor
Optical spectrum analyzer
Output light
PD
frep
RF frequency counter
RF spectrum analyzer
Rb frequency standard
(b)

Fig. 1.

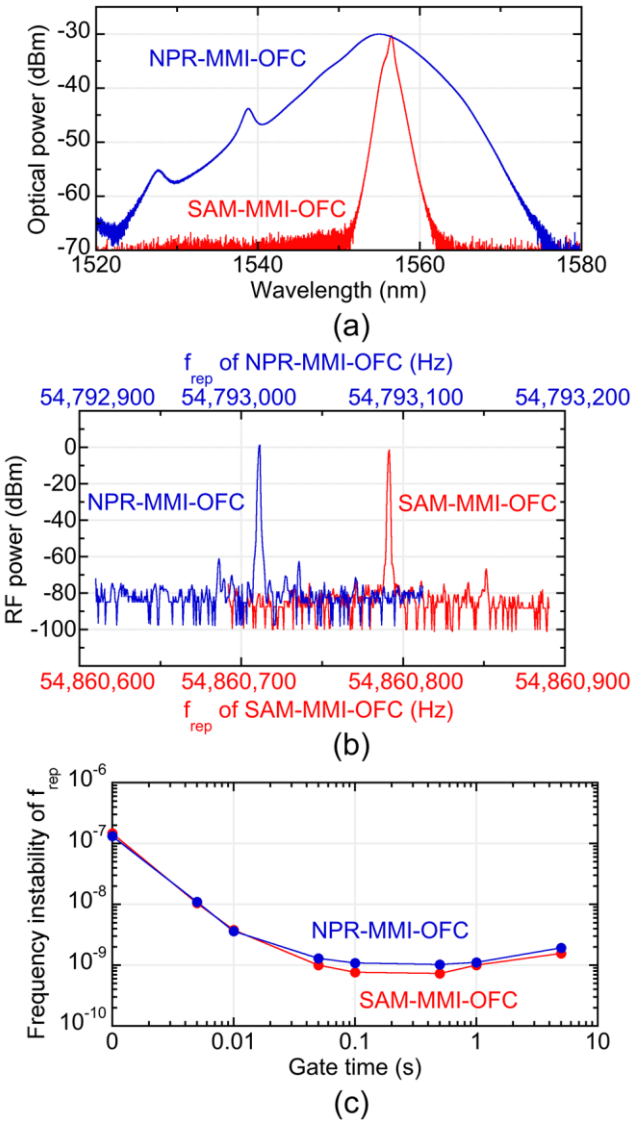
Optical power (dBm)
-30
-40
-50
-60
-70
NPR-MMI-OFC
SAM-MMI-OFC
1520
1540
1560
1580
Wavelength (nm)
(a)
f rep of NPR-MMI-OFC (Hz)
54,792,900
54,793,000
54,793,100
54,793,200
RF power (dBm)
0
-20
-40
-60
-80
-100
NPR-MMI-OFC
SAM-MMI-OFC
54,860,600
54,860,700
54,860,800
54,860,900
f rep of SAM-MMI-OFC (Hz)
(b)
Frequency instability of f rep
10-6
10-7
10-8
10-9
10-10
NPR-MMI-OFC
SAM-MMI-OFC
0
0.01
0.1
1
10
Gate time (s)
(c)

Fig. 2.

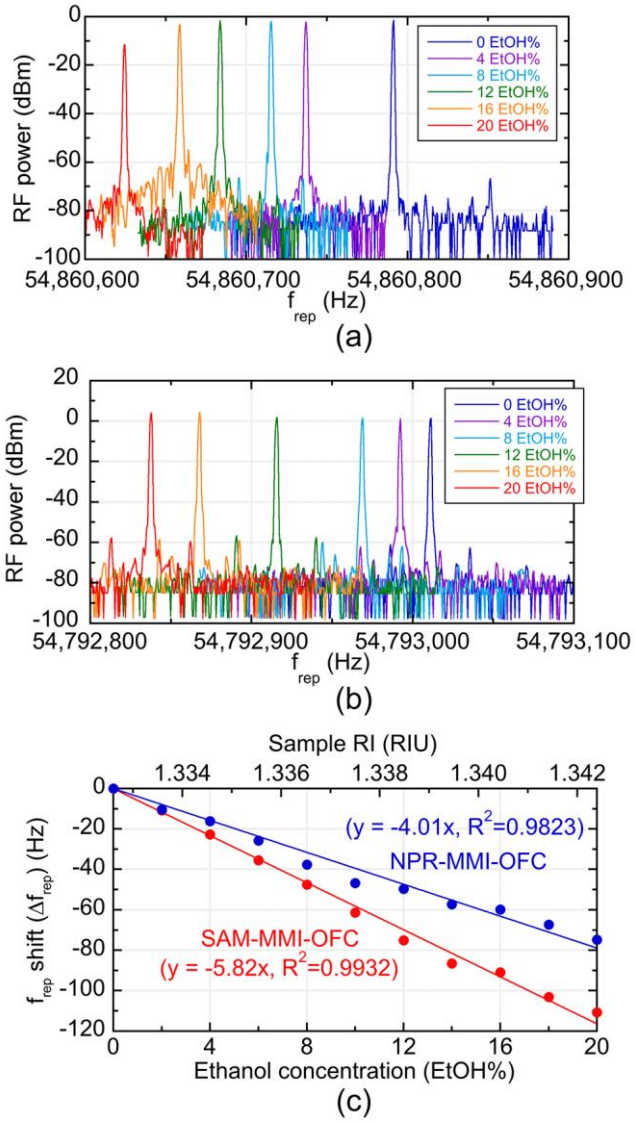
RF power (dBm)
0
-20
-40
-60
-80
-100
54,860,600
54,860,700
54,860,800
54,860,900
f rep (Hz)
0 EtOH%
4 EtOH%
8 EtOH%
12 EtOH%
16 EtOH%
20 EtOH%
(a)
RF power (dBm)
20
0
-20
-40
-60
-80
-100
54,792,800
54,792,900
54,793,000
54,793,100
f rep (Hz)
0 EtOH%
4 EtOH%
8 EtOH%
12 EtOH%
16 EtOH%
20 EtOH%
(b)
Sample RI (RIU)
1.334
1.336
1.338
1.340
1.342
f rep shift (Δf rep) (Hz)
0
-20
-40
-60
-80
-100
-120
(y = -4.01x, R2=0.9823)
NPR-MMI-OFC
SAM-MMI-OFC
(y = -5.82x, R2=0.9932)
0
4
8
12
16
20
Ethanol concentration (EtOH%)
(c)

Fig. 3.

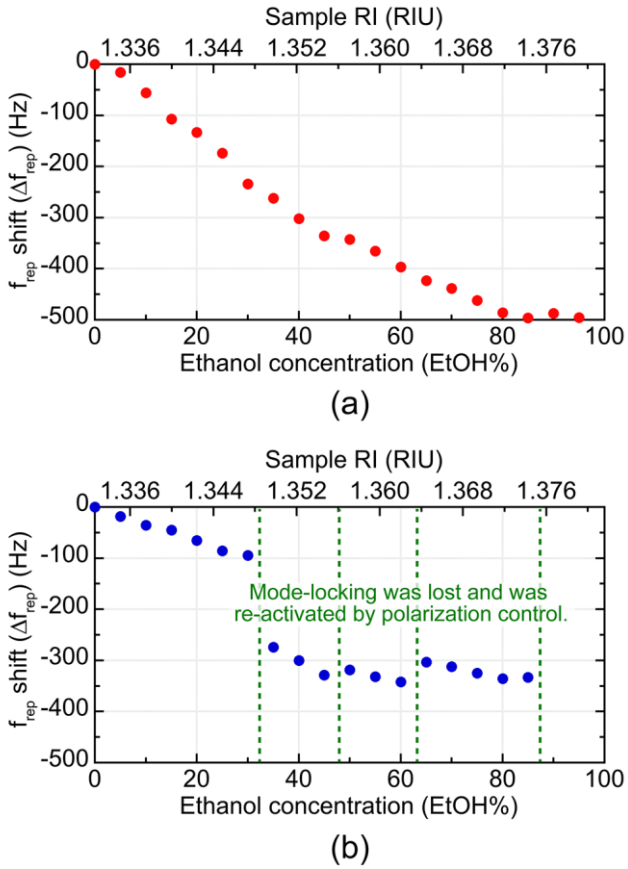
Sample RI (RIU)
1.336
1.344
1.352
1.360
1.368
1.376
0
-100
-200
-300
-400
-500
f_{rep} shift (Δf_{rep}) (Hz)
0
20
40
60
80
100
Ethanol concentration (EtOH%)
(a)
Sample RI (RIU)
Mode-locking was lost and was
re-activated by polarization control.
(b)

Fig. 4.

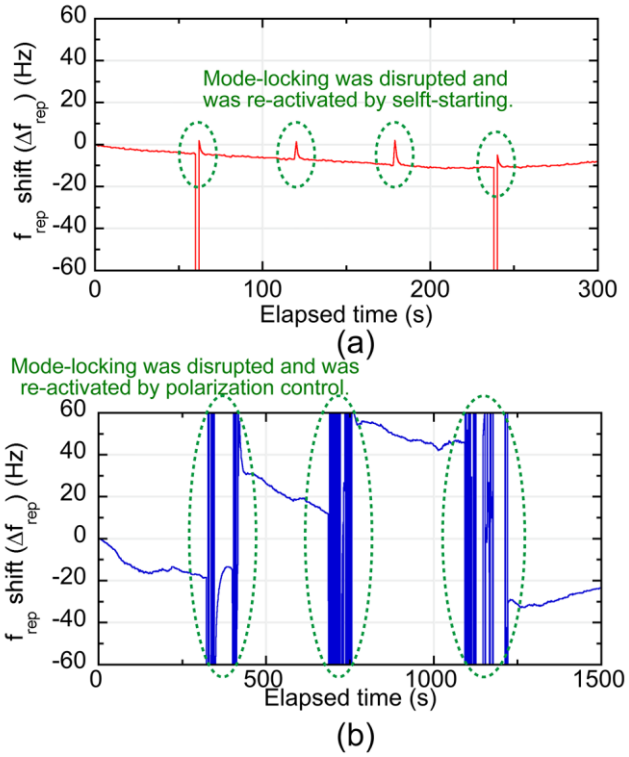
Mode-locking was disrupted and
was re-activated by selft-starting.
f rep shift (Δf rep) (Hz)
Elapsed time (s)
(a)
Mode-locking was disrupted and was
re-activated by polarization control.
f rep shift (Δf rep) (Hz)
Elapsed time (s)
(b)

Fig. 5.